ISSN 0021-3640, JETP Letters, 2013, Vol. 97, No. 8, pp. 447–451. © Pleiades Publishing, Inc., 2013.
Original Russian Text © Yu.S. Ponosov, S.V. Strel'tsov, 2013, published in Pis'ma v Zhurnal Eksperimental'noi i Teoreticheskoi Fiziki, 2013, Vol. 97, No. 8, pp. 517–521.

Q-Dependent Light Scattering by Electrons in LaB_6

Yu. S. Ponosov[a] and S. V. Strel'tsov[a, b]

[a] *Institute of Metal Physics, Ural Branch, Russian Academy of Sciences, ul. S. Kovalevskoi 18, Yekaterinburg, 620990 Russia*
e-mail: ponosov@imp.uran.ru
[b] *Ural Federal University, Yekaterinburg, 620002 Russia*

Received March 18, 2013

The inelastic light scattering by intraband electronic excitations in metallic lanthanum hexaboride has been studied in the temperature range of 10–300 K. General agreement has been obtained between the measured spectra and the spectra calculated within the band theory taking into account the renormalization of electron energies owing to electron–phonon scattering. The electron–phonon coupling constant λ and electron relaxation frequency Γ have been estimated. The dependence of the electron self-energies on the direction and magnitude of the wave vector has been revealed, implying the anisotropic electron–phonon interaction or the contribution from other electron scattering mechanisms.

DOI: 10.1134/S0021364013080122

Investigation of rare-earth hexaborides RB_6 remains topical because of the variety of their physical properties. These hexaborides include metals (LaB_6, YB_6) [1], Kondo insulators (SmB_6) [2], heavy-fermion systems (CeB_6) [3], and magnetic systems (PrB_6, NdB_6) [4]. They all are crystallized into a simple crystal lattice CsCl (space group $O1h$ ($Pm3m$)), where lanthanide atoms are at Cs positions and octahedra of boron atoms occupy Cl positions.

Hexaboride LaB_6 is a superconductor with the transition temperature $T_c \sim 0.1$ K [1]. Owing to a low work function of electrons, it is applied in industry as a source of electrons. Its electronic and lattice properties are well studied. A number of low-temperature anomalies were revealed in the behavior of its electric resistivity, heat conductivity, specific heat, and thermal electron emission [5, 6]. A pseudogap at $T < 100$ K was found in recent photoemission experiments [7]. Different variants of the electron–phonon interaction are proposed as reasons for the observed anomalies. The phonon spectrum of LaB_6 was studied in many Raman studies [8–10]. Despite a number of revealed anomalies (the splitting of degenerate modes and the appearance of forbidden lines), manifestations of any effects of the electron–phonon coupling were not reported in those works.

Inelastic light scattering by electrons can provide information on the structure of the Fermi surface, electron velocities, and electron scattering mechanisms [11, 12]. In this work, we report the first temperature measurements of the light scattering by electrons in LaB_6 depending on the wave vector $\mathbf{q}$. The comparison with the spectra simulated using the calculated Fermi surface with the inclusion of the electron–phonon scattering effects would make it possible to discuss possible reasons for the observed anomalies and to estimate the electron–phonon coupling constant and the electron relaxation frequency.

The measurements were performed on (001) and (011) cleaved facets of a LaB_6 single crystal placed in an optical cryostat. The spectra were excited by lines of argon (488 and 514 nm) and helium–neon (633 nm) lasers. The scattered light was detected in the quasi-backscattering geometry using a Renishaw RM1000 spectrometer equipped with a cooled multichannel CCD detector or a DFS-24 spectrometer equipped with a cooled single-channel photon counter based on a photomultiplier. In the latter case, the laser beam is incident at an angle of 15° to the plane of the sample and the scattered light was collected in the normal direction.

The inset in Fig. 1 shows the Raman spectra of LaB_6 measured at $T = 300$ K for two polarization geometries. In addition to the allowed symmetry phonons T_{2g} (676 cm^{-1}), E_g (1120 cm^{-1}), and A_{1g} (1250 cm^{-1}), a number of other lines (584 cm^{-1}), (747 cm^{-1}), (791 cm^{-1}), (1017 cm^{-1}), (1165 cm^{-1}), (1383 cm^{-1}), and (2215 cm^{-1}) are observed in polarization geometry; most of them can be attributed to two-phonon excitations. The peak near 208 cm^{-1} is likely due to infrared active oscillation T_{1u} from the center of the Brillouin zone, which can become active owing to the finiteness of the wave vector. The phonon lines are imposed on the continuum, which has peaks at low (~300 cm^{-1}) and high (~3000 cm^{-1}) frequencies. The position of a wide high-frequency continuum on the absolute energy scale remains unchanged at a shorter wavelength excitation. Therefore, it is due

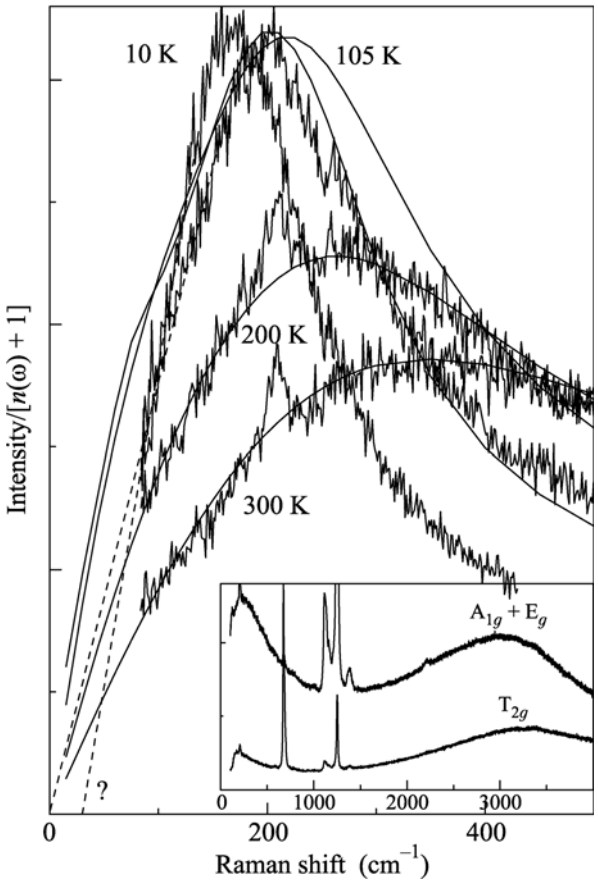

Fig. 1. Spectra of lanthanum hexaboride measured at several temperatures in comparison with the calculations with $\lambda = 0.26$. Excitation is performed at 514 nm and the scattering plane is (011). The inset shows the spectra of LaB_6 measured at $T = 300$ K in a wide frequency range in various polarization geometries.

to luminescence apparently associated with the states of boron because similar luminescence is observed in another hexaboride, SmB_6. This luminescence is observed in LaB_6 for excitation energies above the plasma frequency (2 eV). We attribute the low-energy continuum to inelastic light scattering by electrons, because its frequency varies slightly at different laser excitation energies. Its temperature behavior for excitation at 514 nm (2.41 eV) from the (011) plane is shown in Fig. 1. The pronounced peak near 170 cm^{-1} at 10 K shifts toward higher frequencies and broadens with an increase in the temperature. We previously observed similar scattering in many elementary metals [13–15]. It was interpreted as collisionless light scattering whose cross section is determined by the contribution from all electrons on the Fermi surface and has a maximum at the frequency $\omega = qv_f$, where v_f is the average velocity of electrons and q is the wave vector transfer.

For comparison with the experiment, the frequency dependences of the spectrum of light scattering by intraband electronic excitations were calculated within the polarization operator formalism with allowance for the electron–phonon scattering effects. The frequency dependence of the scattering cross section is determined by the integral of the electronic susceptibility over the distribution of wave vectors (for details, see [14–16]):

$$\chi_{\alpha,\beta}(q,\omega) = \oint \frac{ds_f}{v_f} |\gamma_{\alpha,\beta}(k)|^2 \int_{-\infty}^{\infty} d\epsilon [f(\epsilon) - f(\epsilon+\omega)] \times \Im \frac{1}{\omega - q v_z - \Sigma'(\epsilon+\omega) + \Sigma'(\epsilon) - i[\Sigma''(\epsilon+\omega) + \Sigma''(\epsilon)]}. \quad (1)$$

Here, $\gamma_{\alpha\beta}(k_f, q, \omega)$ is the matrix element of the electron–photon interaction, $f(\epsilon)$ is the Fermi function, v_z is the projection of the velocity on the Fermi surface on the q direction, and $\Sigma(\epsilon)$ and $\Sigma(\epsilon + \omega)$ are the electron self-energies determining the renormalization of the electronic spectrum owing to the electron–phonon scattering in the isotropic approximation [17]. The electronic structure, Fermi surface, and velocities of electrons on the Fermi surface were calculated using the linearized muffin-tin orbital (LMTO) method [18] in the local electron density approximation with an exchange correlation part proposed by von Barth and Hedin [19]. The parameters of the crystal structure of LaB_6 were taken from [20]. A mesh of 125000 k points was used to calculate the electronic susceptibility given by Eq. (1). Empty 4f states of La were considered as a pseudocore [21].

The resulting surface is in agreement with previously calculated surfaces [22, 23] and its extremal dimensions are in agreement with the experimental data [24] within 3%. Hexaboride LaB_6 is a single-band metal. Its Fermi surface consists of six ellipsoids of the 14th band centered at the X points of the Brillouin zone. A small variation of calculation parameters leads to the appearance of small hole surfaces of the 15th band; indications of these surfaces were previously obtained in the experiments reported in [24]. However, their volume is at most 10^{-4} of the volume of the Brillouin zone and their inclusion hardly affects the calculation results. The distribution of wave vector transfers [25] was calculated with the optical data from [26] and the electron–phonon coupling constant was calculated with the phonon density of states $F(\Omega)$ from [27]. The only varying parameter was $\lambda = 2\int d\Omega \alpha^2 F(\Omega)/\Omega$, which determines the electronic self-energies $\Sigma(\omega)$. Its initial value was determined from the estimate of the relaxation frequency $\Gamma \approx 2\Sigma''(\omega)$ at high temperatures. In this case, the collisionless contribution can be neglected and $\chi(\omega)$ can be specified by the following expression for the relaxation mechanism [28]:

$$\chi(\omega) \propto N_f \frac{\omega\Gamma(\omega)}{\omega^2 + \Gamma^2(\omega)}, \quad (2)$$

which gives the maximum of the continuum at the frequency $\omega = \Gamma$ (here, N_f is the density of states at the Fermi level). All calculations were performed with a constant matrix element of the electron–photon interaction.

Although lanthanum hexaboride has a parabolic dispersion law, its Fermi surface is anisotropic. This is one of the reasons responsible for the observation of electronic light scattering; it is commonly accepted [29, 30] that this scattering has a low intensity in the limit $q \longrightarrow 0$ for the scalar component in the nonresonant case. In addition, as will be shown below, the observed scattering is determined by a small nonzero wave vector. The spectra calculated with $\lambda = 0.26$ for several temperatures are shown in Fig. 1 along with the measured spectra whose intensity is divided by $n(\omega) + 1$, where $n(\omega)$ is the Bose–Einstein factor. Agreement with the experiment is satisfactory, but experimental peaks at low temperatures are narrower than the calculated ones. The shape of the spectrum and the position of the maximum are determined by the topology of the Fermi surface and electron velocity distribution. This circumstance makes it possible to estimate the average velocity of electrons as $v_f = 6.5 \times 10^7$ cm/s. The achieved agreement confirms that the observed spectra are really determined by the intraband electronic excitations. The extrapolation of the spectra measured at 10, 30, and 65 K shows that zero intensity is reached at nonzero frequency. However, the situation changes with a further increase in the temperature (Fig. 1). This possibly indicates a decrease in the density of states near the Fermi level at $T < 100$ K, which correlates with the photoemission data reported in [7]. The reported data were obtained using a spectrometer with cutoff filters with a threshold of about 90 cm^{-1}. Owing to this circumstance, the low-frequency range of the spectrum could not be studied in more detail. An increase in the intensity of the spectra measured with excitation at 633 nm (1.96 eV) continued up to the cutoff threshold, preventing an accurate determination of the position of the peak. For this reason, additional measurements were performed at 80 K using a DFS-24 spectrometer with 633-, 514-, and 488-nm excitation lines. As a result, the measurement range was expanded to 20 cm^{-1}. The resulting spectra are shown in Fig. 2 along with the calculated spectra. The optical constants of LaB_6 vary strongly in the visible range of the spectrum. As a consequence, the position of the maximum in the distribution of wave vectors under investigation changes by almost a factor of 3 (see inset in Fig. 2). This change is responsible for the shift of the maximum of the electronic continuum $\omega = qv_f$ with an increase in the excitation energy of the spectrum toward higher frequencies; this behavior is satisfactorily reproduced in the calculation.

The calculations shown in Fig. 2 were performed with the electron–phonon coupling constant $\lambda = 0.26$ for excitation at 514 and 488 nm and with $\lambda = 0.17$ for excitation at 633 nm. Since the expression used for the imaginary part of the electron self-energy $\Sigma''(\omega)$ [16] provides a significant frequency dependence even at room temperature (inset in Fig. 3), the dominance of the relaxation term at high temperatures will assumingly allow the description of electronic continua with a single λ value for any probing wave vector. In this case, the calculation gives almost coinciding positions for continua measured at 300 K with excitation at 633 and 514 nm (the dashed and solid lines in Fig. 3, respectively, calculated with $\lambda = 0.26$). However, although the calculated spectra almost coincide with each other, the position of the continuum for excitation at 633 nm in the experiment is almost 100 cm^{-1} lower. This fact can indicate that electron relaxation frequency can depend not only on the energy but also on the magnitude of the wave vector; this magnitude for excitation at 514 nm is larger than the value for excitation at 633 nm by a factor of 2.5. In order to correctly reproduce the spectrum excited by the 633-nm line, λ was reduced to 0.17. This also gave better agreement with the experiment at $T = 80$ K (Fig. 2).

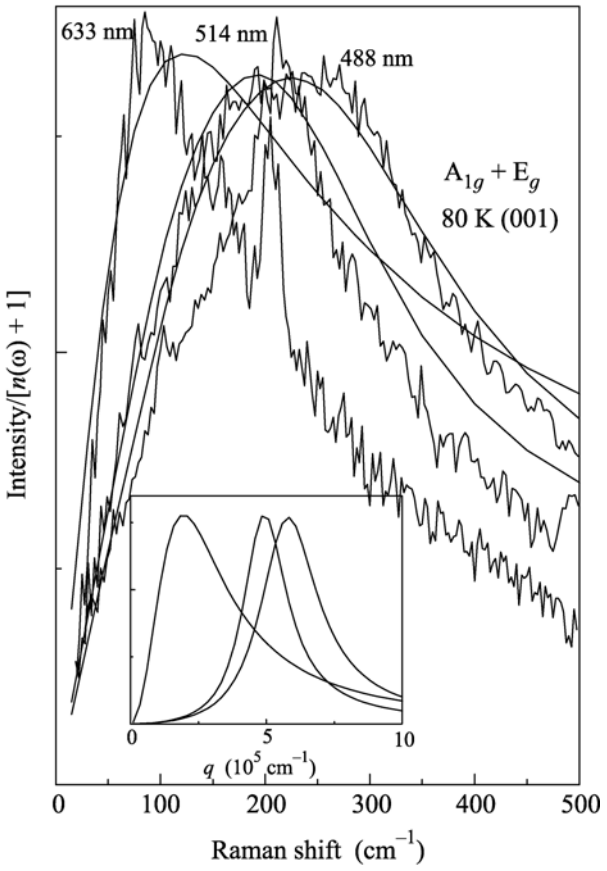

Fig. 2. Spectra measured at 80 K with various excitation lines (indicated near the curves). The inset shows the corresponding distributions of the probing wave vectors for various excitation energies.

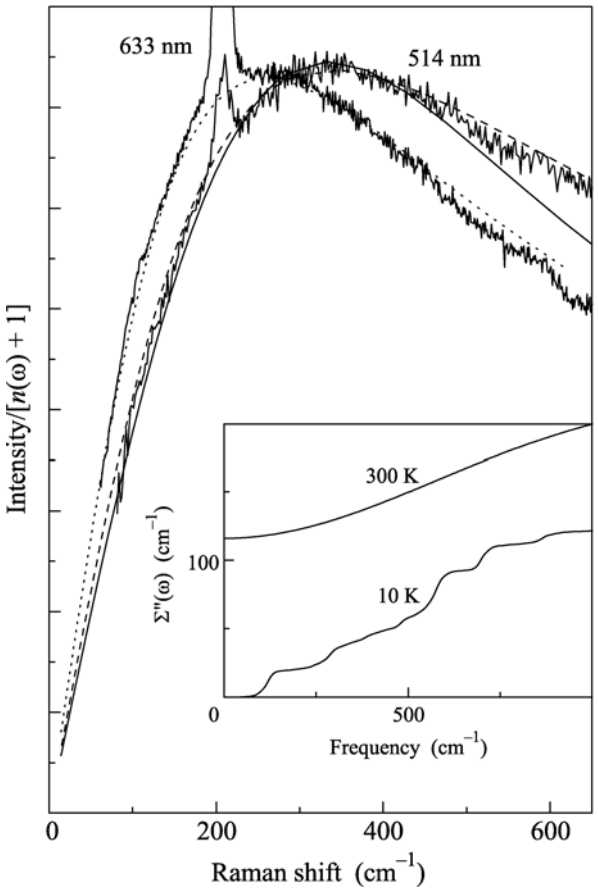

Fig. 3. Spectra measured at 300 K with various excitation lines (indicated near the curves). The solid and dashed lines are the spectra calculated with $\lambda = 0.26$ for excitation at 514 and 633 nm, respectively. The dotted line is the calculation with $\lambda = 0.17$ for 633 nm. The inset shows the frequency dependences $\Sigma''(\omega)$ calculated with $\lambda = 0.26$.

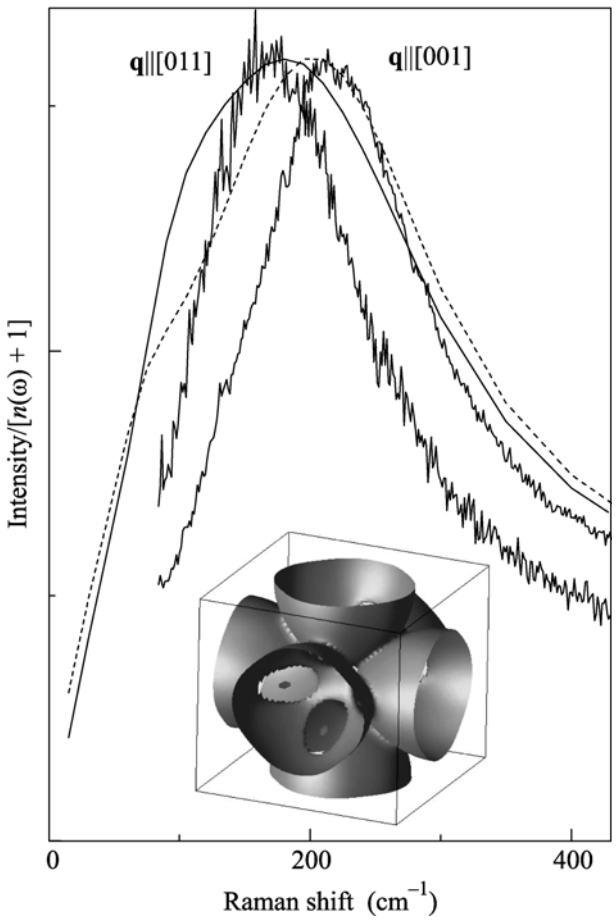

Fig. 4. Spectra measured at 10 K for two directions of the wave vector with excitation at 514 nm. The solid and dashed lines are the calculated spectra for $\mathbf{q} \parallel [001]$ and $\mathbf{q} \parallel [011]$, respectively. The inset shows the calculated Fermi surface.

Another surprising result is demonstrated in Fig. 4, where the spectra measured with excitation at 514 nm for the (001) and (011) crystal planes are shown. The position of the continuum with the wave vector direction $\mathbf{q} \parallel [001]$ in the experiment is shifted by 10–15% toward higher frequencies with respect to the maximum of the continuum with $\mathbf{q} \parallel [011]$. The last fact contradicts the calculated spectra exhibiting the opposite tendency. This can mean a larger renormalization of the mass of the electron for $\mathbf{q} \parallel [011]$ at low temperatures. An increase in the temperature is accompanied by a decrease in the energy difference and the maxima of the continua at room temperature are observed at the same energy.

Our estimates $\lambda = 0.17$–0.26 are somewhat lower than a calculated value of 0.33 [31] and the estimated electron relaxation frequency $\Gamma \sim 260$ cm^{-1} is twice as high as the values obtained from the optical measurements [32]. Comparison of the experimental and calculated spectra confirms that the observed scattering is determined by intraband electronic excitations and the electron–phonon interaction is the main mechanism of the renormalization of the energies of electrons. At the same time, the revealed discrepancies indicate either a strong dependence of the electron–phonon scattering on the magnitude and direction of the wave vector or the existence of additional electron scattering mechanisms. Furthermore, our calculations were performed with the constant matrix element of the electron–photon interaction $\gamma_{\alpha\beta}(k)$, which implies resonance conditions for the entire Fermi surface. The calculation for real resonance conditions can likely lead to a difference between spectra measured with different excitation energies. Moreover, the curvature of the Fermi surface serves as the matrix element in the nonresonant situation [11, 12]. This can possibly lead to a change in the frequencies of the continua for different directions of the momentum. The indicated effects require additional investigations, the more so that rare-earth hexaborides, having a simple electronic spectrum in combination with the possibility of variation of the probing wave vector,

are convenient model objects for detailed studies of the manifestations of the electronic dynamics in light scattering and its changes at the transition from a superconductor with weak coupling (LaB_6 with T_c = 0.1 K) to a superconductor with strong coupling (YB_6 with T_c = 7.5 K) [1].

The samples were prepared at the Laboratory of Refractory Compounds of Rare-Earth Elements, Frantsevich Institute of Materials Science Problems, National Academy of Sciences of Ukraine (Kyiv, Ukraine). Some measurements were performed using the equipment of the Shared Access Center, Faculty of Materials Science, Moscow State University. This work was supported in part by the Russian Foundation for Basic Research (project no. 11-02-00306), by the Ministry of Education and Science of the Russian Federation (project no. 12.740.110026), and by the Council of the President of the Russian Federation for Support of Young Scientists and Leading Scientific Schools (project no. MK-3443.2013.2).

REFERENCES

1. R. J. Sobczak and M. J. Sienko, J. Less-Common Met. **67**, 167 (1979).
2. P. A. Alekseev, J. M. Mignot, J. Rossat-Mignod, et al., J. Phys.: Condens. Matter **7**, 289 (1995).
3. T. Komatsubara, N. Sato, S. Kunii, et al., J. Magn. Magn. Mater. **31–34**, 368 (1983).
4. Y. Onuki, A. Umezawa, W. K. Kwok, et al., Phys. Rev. B **40**, 11195 (1989).
5. D. Mandrus, B. C. Sales, and R. Jin, Phys. Rev. B **64**, 01232 (2001)
6. K. Flachbart, M. Reiffers, S. Janos, et al., J. Less-Common Met. **88**, L3 (1982).
7. V. R. R. Medicherla, S. Patil, R. S. Singh, and K. Maitia, Appl. Phys. Lett. **90**, 062507 (2007).
8. M. Ishii, M. Aono, S. Muranaka, and S. Kawai, Solid State Commun. **20**, 437 (1976).
9. N. Ogita, S. Nagai, N. Okamoto, et al., Phys. Rev. B **68**, 224305 (2003).
10. H. Werheit, V. Filipov, M. Armbruster, and U. Schwarz, Solid State Sci. **14**, 1567 (2012).
11. A. A. Abrikosov and L. A. Fal'kovskii, Sov. Phys. JETP **13**, 179 (1961).
12. I. P. Ipatova, M. I. Kaganov, and A. V. Subashiev, Sov. Phys. JETP **57**, 1066 (1983).
13. Yu. S. Ponosov, G. A. Bolotin, C. Thomsen, and M. Cardona, Phys. Status Solidi B **208**, 257 (1998).
14. Yu. S. Ponosov and S. V. Streltsov, Phys. Rev. B **86**, 045138 (2012).
15. Yu. S. Ponosov and S. V. Streltsov, JETP Lett. **94**, 437 (2011).
16. E. G. Maksimov and S. V. Shulga, Solid State Commun. **97**, 553 (1996).
17. S. V. Shulga, O. V. Dolgov, and E. G. Maksimov, Phys. C **178**, 266 (1991).
18. O. K. Andersen and O. Jepsen, Phys. Rev. Lett. **53**, 2571 (1984).
19. U. von Barth and L. Hedin, J. Phys. C **5**, 1629 (1971).
20. C. H. Booth, J. L. Sarrao, M. F. Hundley, et al., Phys. Rev. B **63**, 2224302 (2001).
21. S. V. Streltsov, A. S. Mylnikova, A. O. Shorikov, et al., Phys. Rev. B **71**, 245114 (2005).
22. A. Hasegawa and A. Yanase, J. Phys. F: Met. Phys. **7**, 1245 (1977).
23. Y. Kubo and S. Asano, Phys. Rev. B **39**, 88228 (1989).
24. H. Harima, O. Sakai, T. Kasuya, and A. Yanase, Solid State Commun. **66**, 603 (1988).
25. A. Dervisch and R. Loudon, J. Phys. C **9**, L669 (1976).
26. P. A. van der Heide, H. W. ten Cate, L. M. ten Dam, et al., J. Phys. F: Met. Phys. **16**, 1617 (1986).
27. T. Gurel and R. Eryigit, Phys. Rev. B **82**, 104302 (2010).
28. A. Zawadowski and M. Cardona, Phys. Rev. B **42**, 10732 (1990).
29. T. P. Devereaux and R. Hackl, Rev. Mod. Phys. **79**, 175 (2007).
30. A. Virosztek and J. Ruvalds, Phys. Rev. Lett. **67**, 1657 (1991); Phys. Rev. B **45**, 347 (1992).
31. G. Schell, H. Winter, H. Rietschel, and F. Gompf, Phys. Rev. B **25**, 1589 (1982).
32. S.-I. Kimura, T. Nanba, S. Kunii, and T. Kasuya, Phys. Rev. B **50**, 1406 (1994).

Translated by R. Tyapaev